Biosensors and Bioelectronics 131 (2019) 113–118

Contents lists available at ScienceDirect

Biosensors and Bioelectronics

journal homepage: www.elsevier.com/locate/bios

A label-free and double recognition–amplification novel strategy for sensitive and accurate carcinoembryonic antigen assay

Zi Liu, Sheng Lei, Lina Zou, Gaiping Li, Lingling Xu, Baoxian Ye*

College of Chemistry and Molecular Engineering, Zhengzhou University, Zhengzhou 450001, PR China

ARTICLE INFO

Keywords:
Dual-function messenger probe
Double recognition-amplification
DNA tetrahedron probes
Hybridization chain reaction
Carcinoembryonic antigen

ABSTRACT

Herein, a label-free and double recognition–amplification (LDRA) strategy for carcinoembryonic antigen (CEA) detection was developed, based on a new designed dual-function messenger probe (DMP) coalescing with DNA tetrahedron probes (DTPs) and hybridization chain reaction (HCR). The DMP possess dual-function to replace CEA for specific interface hybridization and initiate hybridization chain reaction. The interfacial hybridization event was quantitatively converted to an electrochemical signal by using hemin/G-quadruplex (h-Gx) formed after the hybridization chain reaction. Self-assembled DNA tetrahedron probes, which were readily decorated on an electrode surface as a scaffold with rigid support and ordered orientation, enabled the highly efficient strands hybridization and greatly increased target accessibility as well as significantly decreased noise. The proposed assay integrated dual recognition processes and HCR signal amplification processes, achieving the identification of low concentration of CEA as detection limit of 18.2 fg mL^{-1} (S/N = 3) and wider linearity range of 0.0001 ng mL^{-1}–50 ng mL^{-1}. A new electrochemical sensing method was proposed for CEA detection and used in real clinical samples. The obtained results were good consistency with those of clinical diagnosis.

1. Introduction

Cancer, also known as malignant tumor, is one of the major killers to human health and life in modern society (Jayanthi et al., 2017; Wu and Qu, 2015). The levels of tumor markers in tissue or blood often produced higher compared to normal conditions (Akanda and Ju, 2018; Barman et al., 2018; Lee and Zeng, 2017). As a type of acidic glycoprotein, carcinoembryonic antigen (CEA) has closely relationship with cervical carcinoma (Nie et al., 2018; Qiu et al., 2018a), breast cancer, cystadenocarcinoma (Tang et al., 2011; Gu et al., 2018), especially colorectal cancer (Grunnet and Sorensen, 2012; He et al., 2017; Wang et al., 2018a). It is one of the most widely used tumor antigens and commonly monitored in clinic diagnosis and treatment of cancers (Han et al., 2018). Therefore, sensitive and convenient detection of CEA is very crucial for successful prognosis of cancers and the improvement of patient survival. Electrochemical biosensors are widely used in tumor biomarkers detection due to its high sensitivity, easy operation, and real-time monitoring (Chang et al., 2018; Dong et al., 2018; Lv et al., 2018). So far, most electrochemical aptamer-based approaches has been limited to the first-generation or second-generation sensing strategies (Huang et al., 2018), which suffer from shortcomings such as interlacing, interface congestion and high background signals.

DNA is a structure complex organic compound that not only has the function of storing genetic information but also ideal nanomaterials (Chandrasekaran and Levchenko, 2016; Mathur and Medintz, 2017). Due to its high programmability and controllability, it can be used to construct a variety of nano-frame materials by Watson–Crick base pairing rules precisely (Shu et al., 2018; Zhou et al., 2018). Until now, a lot of DNA nanostructures have been assembled with different sizes and shapes (Zhang et al., 2018). Some of them showed excellent applications in the third-generation electrochemical biosensing, which extraordinarily improved the sensitivity and accuracy compared with the first-generation and second-generation electrochemical biosensor (Lin et al., 2014; Zeng et al., 2017). As a classical and simplest polyhedron, DNA tetrahedron probes (DTPs) provide a universal and promising platform to construct a series of electrochemical biosensors (Lin et al., 2016; Wu et al., 2012). DTPs possess unique advantages, including mechanical rigidity and excellent capability of modulating the surface density of the DNA capture probes, which accurately controlling the distance between the probes, avoiding crowding and improving hybridization efficiency (Chen et al., 2014; Ge et al., 2014). In addition, DNA tetrahedron can be easily synthesized by one step, and its high programmability determines its ability to be cleverly designed and combined with other materials (He et al., 2018; Kim et al., 2017; Xie et al., 2016). However, the studies on the application of DTPs in CEA dual recognition detection have been less addressed, which requires

* Corresponding author.
E-mail address: yebx@zzu.edu.cn (B. Ye).

https://doi.org/10.1016/j.bios.2019.02.020
Received 27 November 2018; Received in revised form 15 January 2019; Accepted 4 February 2019
Available online 18 February 2019
0956-5663/

further exploration.

Signal amplification is crucial factor for improving the detection sensitivity in a biosensor assay. For this sake, a variety of signal amplification techniques are induced, such as rolling circle amplification (RCA) (Tian et al., 2018; Yang et al., 2018; Qiu et al., 2018a), polymerase chain reaction (PCR) (Chen et al., 2017; Robinson et al., 2016), catalytic hairpin assembly (CHA) (Karunanayake Mudiyanselage et al., 2018; Li et al., 2017), hybridization chain reaction (HCR) (Ren et al., 2018; Yuan et al., 2018; Qiu et al., 2018b), strand displacement amplification (SDA) (Deng et al., 2018; Dou et al., 2016) and loop-mediated isothermal amplification (LAMP) (Ball et al., 2016; Lee et al., 2016) and so on. HCR is an isothermal, enzyme-free and highly sensitive amplification method, which avoids many limitations of relevant enzymatic way, leading to a widespread application for constructing the sensing platform (Wang et al., 2014). So far, most of the work based on HCR has used marking or auxiliary catalytic materials to realize electron transfer and complete the detection of targets (Chen et al., 2018; Shi et al., 2018). However, the synthesis of labels and materials is cumbersome and difficult to control, which deficiencies complicate the analysis procedure and waste a lot of time and manpower as well as increased cost. Therefore, in this work, hemin/G-quadruplex (h-Gx) was employed to construct a label-free biosensor to further reduce the background signal. The h-Gx is formed by binding a folded G-rich oligonucleotide with a hemin molecule, which can be conveniently generated in situ by various DNA assembly strategies (Hou et al., 2015; Wu et al., 2017). It attracts growing interest, due to the advantages of smaller size, easier functionalization, cheaper operation and more stable under harsh conditions (Yu et al., 2018). In order to improve the sensitivity of the aptasensor, a large amount of h-Gx were accumulated on the electrode by a DNA cyclic HCR method.

In this approach, a label-free and double recognition–amplification (LDRA) strategy for CEA detection was developed with high sensitivity and specificity. In this strategy, we designed a new dual-function messenger probe (DMP). One of its functions was recognized by the C-aptamer, which was fixed on the magnetic beads. When CEA was presence, the equal amount of DMP would be released from MBs and free again. Then, the free DMP was captured by DTPs, which carried the C-aptamer and was self-assembled on a gold electrode surface. Following, the second function of DMP exerted to initiate the HCR from two hairpin probes (H1 and H2). These probes greatly increased target accessibility and minimized the non-specific adsorption due to the rigid scaffold, ordered orientation and well controlled spacing. Thus, the high efficiency and specific hybridization and significantly decreasing noise were received. In the presence of hemin, the G-rich sequence formed after the HCR folded into hemin/G-quadruplex, which produced an electrochemical signal directly. The aptasensor was simple and convenient to construct for nothing complex materials and cumbersome auxiliary catalytic steps were required. The released process of the DMP, including target-specific recognition and specific interface hybridization, as well as the HCR signal amplification process initiated by the DMP, were well integrated into the proposed assay. This strategy successfully reduced the background signal, avoided the false positive signals generated by non-specific adsorption and achieved sensitive detection of CEA. Moreover, the CEA of serum samples from cancer patients were accurately determined by proposed method with good consistency with those of clinical diagnosis.

2. Experimental

2.1. Materials and apparatus

Carcinoembryonic antigen (CEA), hemin, tris (2-carboxyethyl) phosphine hydrochloride (TCEP), ethylenediaminetetraacetic acid (EDTA), thrombin (TB), prostate specific antigen (PSA), hemoglobin (Hb) were purchased from Sigma-Aldrich (St. Louis, MO). 1-ethyl-(3–3′-dimethylaminopropyl) carbodiimide (EDC), N-hydroxysuccinimide (NHS) were purchased from J&KScientific Ltd. (Beijing, China). All HPLC-purified DNA oligonucleotides were purchased from Sangon Biotech Co., Ltd. (Shanghai, China) and dissolved in TE buffer with a concentration of 100 μM. All chemicals were of analytical grade and used when received. Ultrapure water coming from a Millipore system was used throughout the experiments.

The buffer solutions used were prepared as follows: TE buffer: 10 mM tris, 1 mM EDTA, pH 8.0; TM buffer: 20 mM tris and 50 mM $MgCl_2$, pH 8.0; TCEP solution: 100 mM in water; 0.1 M PBS buffer: 0.1 M Na_2HPO_4, 0.1 M NaH_2PO_4, 0.1 M KCl, 0.1 M NaCl, pH 7.0; HEPES buffer: 10 mM HEPES, 10 mM $MgCl_2$, 50 mM NaCl, pH 7.2.

Electrochemical measurements were performed on a CHI-650A electrochemical workstation (Chenhua Instruments Co., Shanghai, China). A three-electrode system was made up of amodified gold electrode (3 mm in diameter) as the working electrode, an Ag/AgCl electrode (saturated KCl) as reference electrode and a Pt wire as counter electrode. Cyclic voltammetry (CV) and electrochemical impedance spectroscopy (EIS) measurement were conducted in the PBS containing 5.0 mM $[Fe(CN)_6]^{3-/4-}$ as redox probe and KCl (0.1 M) as supporting electrolyte. EIS conditions: initial potential of 5 mV; frequency range from 0.1 Hz to100KHz; amplitude of 5 mV. The differential pulse voltammetry (DPV) experiments were performed in 2 mL HEPES (pH 7.2). DPV conditions: potential range from 0–0.6 V; modulation amplitude of 0.05 V; pulse width of 0.05 s; sample width of 0.0167 s.

2.2. Preparation of DMP/C-aptamer/MBs bioconjugates

The C-aptamer and DMP were immobilized on the magnetic beads (MBs) using amide-coupling method (Dong et al., 2018; Yu et al., 2016), described briefly as follows. 500 mL carboxyl-modified MBs in a 5 mL eppendorf tube was separated magnetically. The MBs were washed with 0.1 M PBS (pH 7.0, 3 × 300 μL). Then, 0.8 M EDC solution (200 μL) and 0.4 M NHS solution (200 μL) were added to the eppendorf tube to active the carboxylate at room temperature for 0.5 h. After washing with PBS, MBs were mixed with 1 μM C-aptamer to obtain C-aptamer/MBs by gentle shaking at 37 °C overnight. Then, the unbound C-aptamers were removed via a magnetic separation. Finally, 1 μM DMP was introduced to hybridize with C-aptamer/MBs at 37 °C to obtain the DMP/C-aptamer/MBs. The excess DMP was magnetically separated, and the DMP/C-aptamer/MBs bioconjugates were dispersed in 2 mL PBS and stored at 4 °C for further use.

2.3. Self-assembly of DTPs on gold electrode surfaces

Equal concentrations of four DNA single strands (A, B, C, D; sequences in Table S1) in TM buffer (20 mM Tris-HCl, 50 mM $MgCl_2$, pH 8.0) were first mixed with 30 mM TCEP. Here, TCEP was used to cut the S–S bond. Then, the mixture was heated to 95 °C for 5 min, and then cooled down to room temperature. Gold electrode (3 mm in diameter) was firstly immersed in piranha solution (98% H_2SO_4:30% H_2O_2 = 3:1) for about 30 min. Subsequently, the electrode was treated with 1, 0.3, 0.05 μm alumina slurry. Next, it was cleaned by ultrasonication for 2 min in ethanol and pure water, respectively. Then the electrodes were electrochemically cleaned in a freshly prepared 0.5 M H_2SO_4 solution. After that, 5 μL DTPs (0.5 μM) was dropped on the cleaned electrode surface immediately, and then kept in dark overnight. At the same time, the hairpin probes H1 and H2 were annealed, and stored in 4 °C for further use.

2.4. Native gel electrophoresis

All oligonucleotide samples were heated to 95 °C for 5 min, and then cooled down to room temperature for 2 h before use. All samples were prepared as a concentration of 1 μM. Then 20 μL of each sample was subjected to gel electrophoresis in 2.5% agarose gels at 100 V for 45 min and then strained with GelRed. Image was visualized under UV

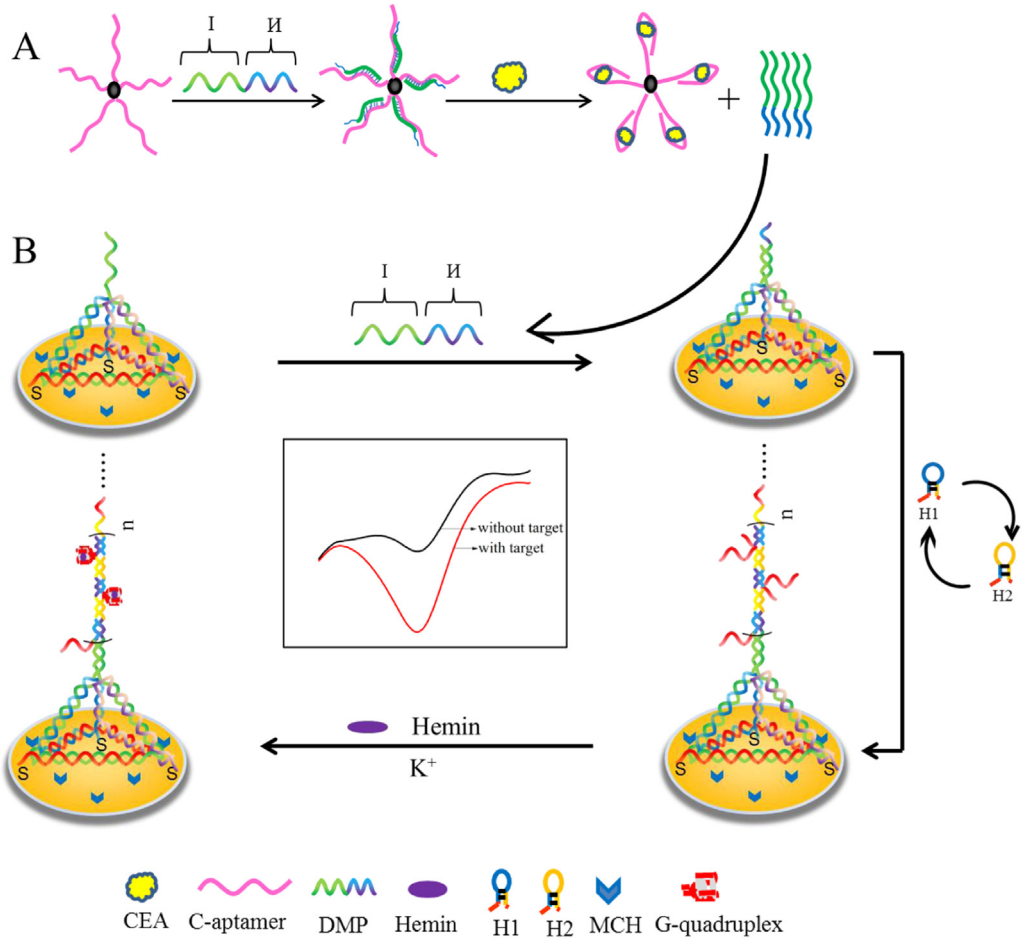

Scheme 1. Schematic illustration of a label-free and double recognition-amplification (LDRA) electrochemical assay for CEA with high sensitivity specificity based on the DNA tetrahedron probes (DTPs) and hybridization chain reaction (HCR) strategy. (A) Specific recognition of target and release of DMP. (B) DMP replaces CEA for accurate identification of heterogeneous interfaces and initiates a HCR to load a large number of h-Gxs to output current signals.

light.

3. Results and discussion

3.1. Design strategy

The working principle of this strategy was shown in Scheme 1. A new dual-function messenger probe (DMP, sequence see Supplementary materials Table 1) was designed elaborately and used to indirectly recognize carcinoembryonic antigen (CEA) and initiated hybridization chain reaction. The two face of DMP were part I and part И. Part I could hybridized with the CEA aptamer (C-aptamer); part И was used to initiate the hybridization chain reaction between hairpin probes H1 and H2. Firstly, we immobilized DMP on the surface of magnetic nanoparticles (MB) modified with C-aptamer (step A). Since the binding force of CEA to C-aptamer was stronger than that between DMP and C-aptamer, when CEA was present, C-aptamer would preferentially bind to it, which completed a specific recognition, and released DMP simultaneously and equivalently. Subsequently, the part I of DMP hybridized with the DNA tetrahedron probes (DTPs), which were modified on the electrode surface in step B. An accurate recognition was finished. Then, an equal amount of two hairpin probes (H1 and H2) were added to the electrode surface. Hybridization chain reaction (HCR) was initiated by the part И of DMP with hybridizing H1, going on between H1 and H2. After that, a long double strand DNA with G-rich sequence branches was formed. In the presence of hemin and K^+, hemin/G-quadruplex was formed, and provided electrochemical signal directly. The employment of DTPs adjusted the density of the probe on the electrode surface, controlled the distance and orientation, increased the probability of hybridization, and reduced the background signal. The synergetic combination of dual recognition function of the DMP and the signal amplification function of HCR decreased the interference of non-specific amplification and adsorption, effectively avoided the generation of false positive signals and improved the detection sensitivity for CEA.

3.2. Characterization of aptasensing interface

The stepwise assembly process of the aptasensor interface was identified by cyclic voltammetry (CV) and electrochemical impedance spectroscopy (EIS) techniques. From the Fig. 1A, we could see that a well-defined redox peak from $[Fe(CN)_6]^{3-/4-}$ was observed at the bare Au electrode (curve a). After DNA tetrahedron probe immobilized on the electrode surface, the negatively charged phosphate backbone of DTPs rejected the diffusion of $[Fe(CN)_6]^{3-/4-}$ redox probe toward electrode surface, leading to the peak current markedly decreased (curve b). The assembly of MCH also yielded a decrease in current intensity (curve c). This may derived from the influence of MCH which had the function of blocking electron transfer rate. With the combination of CEA and aptamer, the DMP was released from the MBs and hybridized with the erect part of DTPs, which aggrandized the electrostatic repulsive force of $[Fe(CN)_6]^{3-/4-}$ solution, so the electrochemical signal response reduced (curve d). After HCR procedure, a long DNA duplex and hemin/G-quadruplex was formed and the peak current reduced again (curve e).

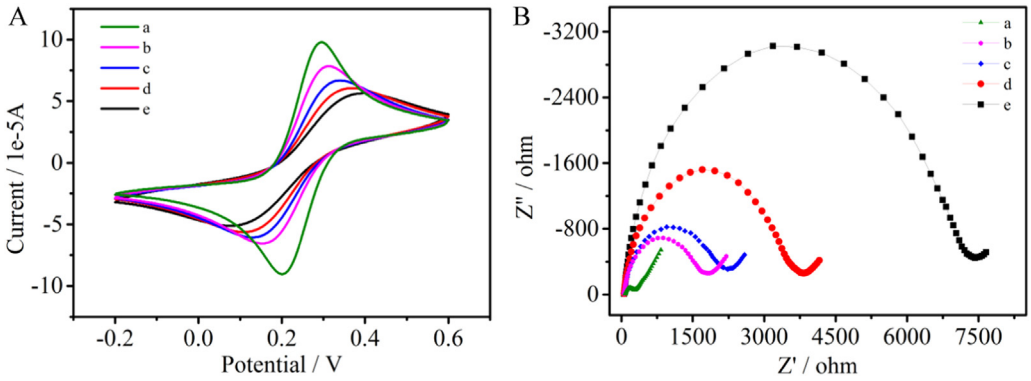

Fig. 1. (A) Cyclic voltammograms and (B) Nyquist plots of biosensor with stepwise assembly process in PBS containing 5 mM $[Fe(CN)_6]^{3-/4-}$: (a) bare Au, (b) DTPs/Au, (c) MCH/DTPs/Au, (d) DMP/MCH/DTPs/Au, (e) hemin/H1-H2/DMP/MCH/DTPs/Au. (EIS conditions: initial potential of 5 mV; frequency range from 0.1 Hz to 100 KHz; amplitude of 5 mV.).

The consistent experiment results were revealed by the EIS measurements (Fig. 1B). We also investigated that an obvious current signal provided by hemin was generated only in the presence of the target (see Supplementary materials S1).

3.3. Characterization of DTPs and HCR

The results of agarose gel electrophoresis for DTPs and HCR were illustrated in Fig. 2. DTPs were self-assembly of four single strands. Among them, one of the sequences was designed with aptamer for the capture of DMP, while the other three were modified with thiol at terminal used to anchor the DTPs on the electrode surface. As shown in Fig. 2., lane 1 represents DNA maker. The assembled DTPs (lane 2) moved more slowly than other combination formed by less than four oligonucleotides (lane 3, 4, 5), which suggested the successful assembly of DTPs. As seen from lane 6, one clear bands corresponding to H1. In the absence of the target, DMP would remained on the MB while the two hairpins remain folded in solution, indicated that no hybridization was occurred. Therefore, only one band could be found in Fig. 2. (lane 7). However, in the present of target, the initiator, DMP, will be released from MBs. The steady state was disturbed by the hybridization of DMP and H1 and several bands were received when H1 and H2 were simultaneously mixed in the incubation solution (lane 8). Finally, the hybridization chain reaction would stopped, when the supply of the two hairpins was exhausted. This whole phenomenon indicated the successful self-assembly of DTPs and the smooth occurrence of HCR.

3.4. Optimization of experimental condition

In order to obtain the best performance for detecting CEA, the experimental conditions were optimized one by one, including the concentration of DTPs, the binding time of CEA and C-aptamer, and the reaction time of HCR. We first optimized the incubation time of target (30 nM) and detected by DPV. As illustrated in Fig. 3A, the current intensity showed a rapid increase with augment of incubation time from 10 min to 70 min and nearly kept stable after 70 min. The result indicated that a saturation of binding between CEA and C-aptamer was achieved at this point. That is to say, the optimal incubation time was 70 min in the electrochemical sensing system. Furthermore, the concentration of DTPs concentration was investigated by CV with $[Fe(CN)_6]^{3-/4-}$ (5.0 mM) as redox probe. As illustrated in Fig. 3B, the current decreased from 0 to 0.4 μM and kept stable after 0.4 μM, which indicated that the DTPs modified on the electrode surface reached saturation. In order to facilitate calculations, 0.5 μM DTPs was chosen in the following experiment. HCR reaction time played an important role in the production of longer dsDNA strands, which directly affected the adsorption of hemin. Therefore, the effect of HCR reaction time on current signal was also studied. 5 μL 1 μM H1 and H2 solution was dropped on the electrode surface and incubated for 30 min, 60 min, 90 min, 120 min, 150 min and 180 min, respectively. Then, DPV measurements were performed in HEPES buffer (pH 7.2). As shown in Fig. 3C, the current intensity increased with time, and tended to steady after 120 min. Hence, 120 min was chosen as the optimized hybridization time for HCR. The results showed that the optimal concentration of DTP, the binding time of CEA and C-aptamer as well as the reaction time of HCR were 0.5 μM, 70 min and 120 min, respectively.

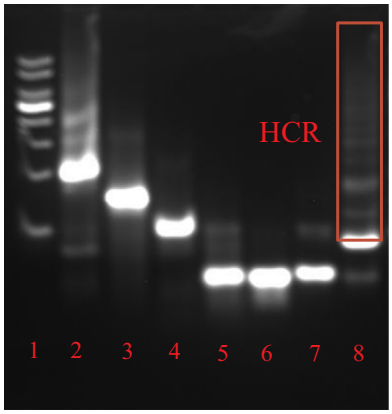

Fig. 2. Analysis by agarose gels: lane 1: maker, lane 2: DTPs (A + B + C + D), lane 3: A + B + C, lane 4: B + D, lane 5: C, lane 6: H1, lane 7: HCR process in the absence of CEA, lane 8: HCR in the presence of CEA.

3.5. Quantification of CEA

Under the optimal conditions, the aptasensors were incubated in the solutions with different concentrations of CEA, and the DPV responses of the proposed aptasensors were recorded. A superimposed DPV curves was shown in Fig. 4A with CEA concentrations ranging from 0.1 pg/mL to 50 ng/mL. Distinctly, the reduction peak currents increased with increasing CEA concentrations. The Fig. 4B displayed a well linear relation between the peak currents and the logarithm of CEA concentrations according linear equation of $I_p = -0.377 \log C - 1.909$ ($R^2 = 99.39\%$) with a detection limit of 18.2 fg/mL (S/N = 3). Hence, the proposed strategy and method could be used to quantification of CEA with high sensitivity and wider detection linear range. A comparison of proposed method with other approaches was listed in Table 1. In addition, the proposed method was much simpler operation.

3.6. The selectivity, reproducibility of the biosensor

A pivotal issue was the specificity of the proposed strategy. To assess the potential of the aptasensor to differentiate target from complex samples, PSA, TB, and Hb with concentrations 10-fold higher than that of CEA (30 ng/mL) were chosen as potential rivals to this aptasensor. As shown in Fig. 5, only in the presence of CEA did the aptasensor exhibit an obvious electrochemical signal. Even if the competitors were 10-fold

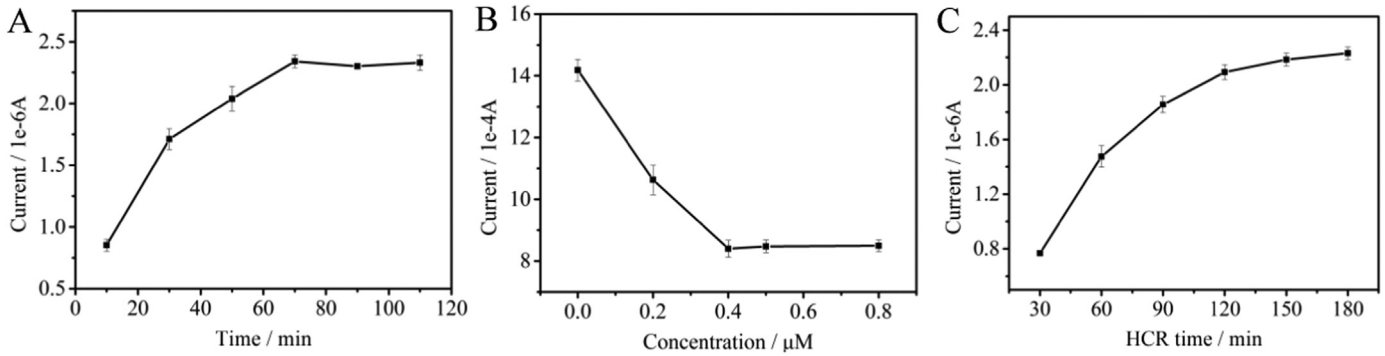

Fig. 3. (A) The time optimization of CEA incubation, the studied time were 10, 30, 50, 70, 90 and 110 min, respectively. (B) Optimization DTPs density on the electrode surface: 0, 0.2, 0.4, 0.5 and 0.8 μM, respectively. (C) The effect of HCR time of H1 and H2: 30, 60, 90, 120, 150 and 180 min, respectively. The concentration of CEA used in A–C was 30 ng/mL. Error bars show standard deviations of three repetitive measurements.

larger than CEA, it had a negligible effect on the current signal compared to the blank test. This suggested that the proposed aptasensor could specifically identified CEA in the co-existence of interfering protein. The reproducibility of this aptasensor was also investigated. Six independent electrodes were used under the same condition to detect CEA (30 ng/mL), all the statistics implicated a similar electrochemical response, and the relative standard deviation (RSD) was 4.37%. This result indicated a good reproducibility of the proposed aptasensor.

3.7. Quantification of CEA in human serum sample

In order to evaluating the feasibility of the developed method for CEA detection, the practical flexibility was carried out in human serum sample (obtained from the First Affiliated Hospital of Zhengzhou University, China). Five real samples were chosen and analyzed by the proposed aptasensor. The results were list in Table S2. The results were compared with that from the electrochemiluminescence (ECL) method adopted by the hospital. (See Supplementary materials Table S2). It could be seen that the relative deviations between the two methods were from −2.3–5.42%, indicated the proposed strategy was in good agreement with ECL method and easier to operate. Thus, the proposed strategy may provide an interesting alternative tool for the detection of CEA in clinical diagnosis.

4. Conclusion

In this work, an electrochemical assay for CEA detection with high sensitivity and specificity was reported based on a new dual-function messenger probe (DMP) and label free double recognition-amplification strategy. The significant merits were ascribed to the integration of double recognition-amplification processes, embodied in DMP released from MBs and replaced the CEA for specific interface hybridization, as well as HCR signal amplification processes. Accurate recognition of interface nanostructure probes and DMP significantly improved the S/B ratio, effectively avoided the interference caused by the entanglement of the single-chain aptamer probe on the current signal. In addition, this strategy effectively reduced the background signal, improved the detection sensitivity and achieved a detection limit as low as 18.2 fg/mL. For electrode surface modification, multiple operation steps were required (e.g., washing and binding steps) compared to traditional ELISA method. Therefore, it is of great necessity to develop washing free and automatic detection strategy for the target, which is our effort in the future.

CRediT authorship contribution statement

Zi Liu: Conceptualization, Methodology, Validation, Formal analysis, Investigation, Resources, Data curation, Writing - original draft, Writing - review & editing. **Sheng Lei:** Validation, Formal analysis, Methodology, Investigation. **Lina Zou:** Formal analysis, Methodology, Investigation. **Gaiping Li:** Formal analysis, Investigation. **Lingling Xu:** Investigation. **Baoxian Ye:** Data curation, Writing - review & editing, Project administration.

Acknowledgments

The authors are sincerely grateful for the financial support from the National Natural Science Foundation of China (No. 21575130).

Declaration of interests

None.

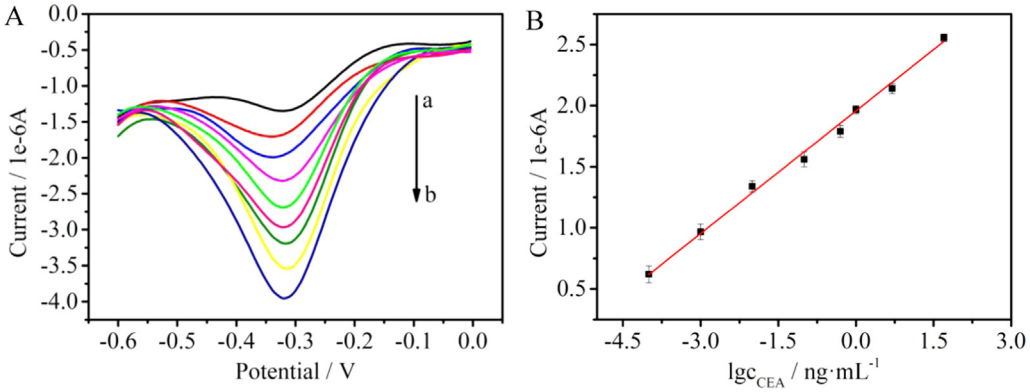

Fig. 4. (A) Superimposed DPV curves with different CEA concentrations in 10 mM HEPES (pH 7.2). From a to b: 0 pg/mL, 0.1 pg/mL, 1 pg/mL, 10 pg/mL, 100 pg/mL, 0.5 ng/mL, 1 ng/mL, 5 ng/mL, 50 ng/mL. (B) The calibration plots of current intensity versus the logarithm of target CEA concentrations. (Error bars, SD; n = 3).

Table 1
Analytical performances of different methods for CEA detection.

Method	Detection range (ng/mL)	detection limit (pg/mL)	References
Electrochemiluminescence	0.001–500	0.17	Wang et al. (2018a)
Fluorescence	0.01–100	1.2	He et al. (2017)
Fluorescence	0.05–20	6.7	Qiu et al. (2017)
Electrochemical immunoassay	0.05–20	10	Gu et al. (2018)
Electrochemical immunoassay	0.01–80	1.0	Tang et al. (2011)
Electrochemical immunoassay	0.0001–20	0.03	Wang et al. (2018b)
Electrochemical immunoassay	0.001–120	0.5	Zhou et al. (2012)
Photoelectrochemical	0.01–50	3.2	Han et al. (2018)
Photoelectrochemical	0.0005–50	0.14	Nie et al. (2018)
Photoelectrochemical	0.01–40	3.6	Qiu et al. (2018a)
Photoelectrochemical	0.005–5.0	1.9	Qiu et al. (2018b)
Electrochemical	0.0001–50	0.0182	This work

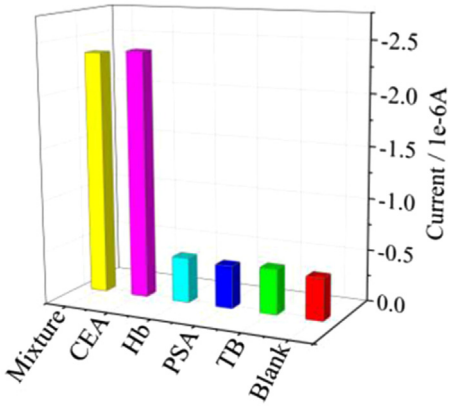

Fig. 5. Histograms of the selectivity of the aptasensor examined by being incubated in the following samples under the same experimental conditions. The concentration of CEA was 30 ng/mL and other interferences were 300 ng/mL.

Appendix A. Supporting information

Supplementary data associated with this article can be found in the online version at https://doi.org/10.1016/j.bios.2019.02.020.

References

Akanda, M.R., Ju, H.X., 2018. Anal. Chem. 90, 8028–8034.
Ball, C.S., Light, Y.K., Koh, C.Y., Wheeler, S.S., Coffey, L.L., Meagher, R.J., 2016. Anal. Chem. 88, 3562–3568.
Barman, S.C., Hossain, M.F., Yoon, H., Park, J.Y., 2018. Biosens. Bioelectron. 100, 16–22.
Chandrasekaran, A.R., Levchenko, O., 2016. Chem. Mater. 28, 5569–5581.
Chang, Y.Y., Li, M.Y., Wu, Z.Y., Zhuo, Y., Chai, Y.Q., Xiao, Q., Yuan, R., 2018. Anal. Chem. 90, 8241–8247.
Chen, F., Wang, X.Y., Cao, X.W., Zhao, Y.X., 2017. Anal. Chem. 89, 10468–10473.
Chen, X.Q., Zhou, G.B., Song, P., Wang, J.J., Gao, J.M., Lu, J.X., Fan, C.H., Zuo, X.L., 2014. Anal. Chem. 86, 7337–7342.
Chen, Y.X., Huang, K.J., He, L.L., Wang, Y.H., 2018. Biosens. Bioelectron. 100, 274–281.
Deng, X.L., Wang, C., Gao, Y., Li, J.W., Wen, W., Zhang, X.H., Wang, S.F., 2018. Biosens. Bioelectron. 105, 211–217.
Dong, H.L., Chen, H.F., Jiang, J.Q., Zhang, H., Cai, C.X., Shen, Q.M., 2018. Anal. Chem. 90, 4507–4513.
Dou, B.T., Yang, J.M., Shi, K., Yuan, R., Xiang, Y., 2016. Biosens. Bioelectron. 83, 156–161.
Ge, Z.L., Lin, M.H., Wang, P., Pei, H., Yan, J., Shi, J.Y., Huang, Q., He, D.N., Fan, C.H., Zuo, X.L., 2014. Anal. Chem. 86, 2124–2130.
Grunnet, M., Sorensen, J.B., 2012. Lung Cancer 76, 138–143.
Gu, X.F., She, Z., Ma, T.X., Tian, S., Kraatz, H.B., 2018. Biosens. Bioelectron. 102, 610–616.
Han, Q.Z., Wang, R.Y., Xing, B., Zhang, T., Khan, M.S., Wu, D., Wei, Q., 2018. Biosens. Bioelectron. 99, 493–499.
He, L., Lu, D.Q., Liang, H., Xie, S.T., Zhang, X.B., Liu, Q.L., Yuan, Q., Tan, W.H., 2018. J. Am. Chem. Soc. 140, 258–263.
He, M.Q., Wang, K., Wang, W.J., Yu, Y.L., Wang, J.H., 2017. Anal. Chem. 89, 9292–9298.
Hou, T., Li, W., Liu, X.J., Li, F., 2015. Anal. Chem. 87, 11368–11374.
Huang, J.Y., Zhao, L., Lei, W., Wen, W., Wang, Y.J., Bao, T., Xiong, H.Y., Zhang, X.H., Wang, S.F., 2018. Biosens. Bioelectron. 99, 28–33.
Jayanthi, V., Das, A.B., Saxena, U., 2017. Biosens. Bioelectron. 91, 15–23.
Karunanayake Mudiyanselage, A., Yu, Q.K., Leon-Duque, M.A., Zhao, B., Wu, R., You, M.X., 2018. J. Am. Chem. Soc. 140, 8739–8745.
Kim, S.H., Kim, K.R., Ahn, D.R., Lee, J.E., Yang, E.G., Kim, S.Y., 2017. ACS Nano 11, 9352–9359.
Lee, D., Kim, Y.T., Lee, J.W., Kim, D.H., Seo, T.S., 2016. Biosens. Bioelectron. 79, 273–279.
Lee, K.H., Zeng, H.Q., 2017. Anal. Chem. 89, 12743–12748.
Li, X., Xie, J.Q., Jiang, B.Y., Yuan, R., Xiang, Y., 2017. ACS Appl. Mater. Interfaces 9, 5733–5738.
Lin, M.H., Wen, Y.L., Li, L.Y., Pei, H., Liu, G., Song, H.Y., Zuo, X.L., Fan, C.H., Huang, Q., 2014. Anal. Chem. 86, 2285–2288.
Lin, M.H., Song, P., Zhou, G.B., Zuo, X.L., Aldalbahi, A., Lou, X.D., Shi, J.Y., Fan, C.H., 2016. Nat. Protoc. 11, 1244–1263.
Lv, S.Z., Zhang, K.Y., Zeng, Y.Y., Tang, D.P., 2018. Anal. Chem. 90, 7086–7093.
Mathur, D., Medintz, I.L., 2017. Anal. Chem. 89, 2646–2663.
Nie, G.M., Tang, Y., Zhang, B., Wang, Y., Guo, Q.F., 2018. Biosens. Bioelectron. 116, 60–66.
Qiu, Z.L., Shu, J., Tang, D.P., 2017. Anal. Chem. 89, 5152–5160.
Qiu, Z.L., Shu, J., Tang, D.P., 2018a. Anal. Chem. 90, 1021–1028.
Qiu, Z.L., Shu, J., Tang, D.P., 2018b. Anal. Chem. 90, 12214–12220.
Ren, K.W., Xu, Y.F., Liu, Y., Yang, M., Ju, H.X., 2018. ACS Nano 12, 263–271.
Robinson, P.V., Tsai, C.T., de Groot, A.E., McKechnie, J.L., Bertozzi, C.R., 2016. J. Am. Chem. Soc. 138, 10722–10725.
Shi, X.M., Fan, G.C., Tang, X., Shen, Q., Zhu, J.J., 2018. Biosens. Bioelectron. 109, 190–196.
Shu, J., Qiu, Z.L., Lv, S.Z., Zhang, K.Y., Tang, D.P., 2018. Anal. Chem. 90, 2425–2429.
Tang, J., Tang, D.P., Niessner, R., Chen, G.N., Kopp, D., 2011. Anal. Chem. 83, 5407–5414.
Tian, B., Qiu, Z., Ma, J., Donolato, M., Hansen, M.F., Svedlindh, P., Stromberg, M., 2018. ACS Appl. Mater. Interfaces 10, 2957–2964.
Wang, F., Lu, C.H., Willner, I., 2014. Chem. Rev. 114, 2881–2941.
Wang, N.N., Feng, Y.Q., Wang, Y.W., Ju, H.X., Yan, F., 2018a. Anal. Chem. 90, 7708–7714.
Wang, Y.G., Zhao, G.H., Zhang, Y., Pang, X.H., Cao, W., 2018b. Sens. Actuators B-Chem. 266, 561–569.
Wu, L., Qu, X.G., 2015. Chem. Soc. Rev. 44, 2963–2997.
Wu, Y.L., Pei, H., Shen, Y., Xi, J.J., Lin, M.H., Lu, N., Shen, X.Z., Li, J., Fan, C.H., 2012. Sci. Rep. 11, 1244–1263.
Wu, Y.M., Zou, L.N., Lei, S., Yu, Q., Ye, B.X., 2017. Biosens. Bioelectron. 97, 317–324.
Xie, S.B., Dong, Y.W., Yuan, Y.L., Chai, Y.Q., Yuan, R., 2016. Anal. Chem. 88, 5218–5224.
Yang, X.J., Zhang, K., Xu, J.J., Chen, H.Y., 2018. Anal. Chem. 90, 6199–6205.
Yu, Q., Wu, Y.M., Liu, Z., Lei, S., Li, G.P., Ye, B.X., 2018. Biosens. Bioelectron. 107, 178–183.
Yu, T., Dai, P.P., Xu, J.J., Chen, H.Y., 2016. ACS Appl. Mater. Interfaces 8, 4434–4441.
Yuan, B.Y., Chen, Y.Y., Sun, Y.Q., Guo, Q.P., Huang, J., Liu, J.B., Meng, X.X., Yang, X.H., Wen, X.H., Li, Z.H., Li, L., Wang, K.M., 2018. Anal. Chem. 90, 6131–6137.
Zeng, D.D., Wang, Z.H., Meng, Z.Q., Wang, P., San, L.L., Wang, W., Aldalbahi, A., Li, L., Shen, J.W., Mi, X.Q., 2017. ACS Appl. Mater. Interfaces 9, 24118–24125.
Zhang, K.Y., Lv, S.Z., Lin, Z.Z., Li, M.J., Tang, D.P., 2018. Biosens. Bioelectron. 101, 159–166.
Zhou, J., Tang, D.P., Hou, L., Cui, Y.L., Chen, G.N., 2012. Anal. Chim. Acta 751, 52–58.
Zhou, Q., Lin, Y.X., Zhang, K.Y., Li, M.J., Tang, D.P., 2018. Biosens. Bioelectron. 101, 146–152.